Proceedings of the 21st ICSMGE, Vienna, Austria, 14 – 19 June 2026. Pistrol, Adam & Schweiger (eds.)
Published by: ÖGG, Austrian Society for Geomechanics, Salzburg, Austria, ISBN 978-3-9503898-4-5
https://doi.org/10.53243/ICSMGE2026-2220

Evaluation of the compacted embankment zone using shear wave velocity

Younggeun Yoo, Jong-Sub Lee, Dong Geun Son
School of Civil, Environmental and Architectural Engineering, Korea University, Republic of Korea

Junghee Park
Department of Civil and Environmental Engineering, Incheon National University, Republic of Korea, junghee.park@inu.ac.kr

ABSTRACT: Field compaction is a primary consideration in ensuring the long-term stability of civil structures subject to monitoring. In this study, we compact the embankment layers to explore the density of the target ground. The compaction zone is divided into three sections based on relative compaction R_C = 80%, 90%, and 95%, while the non-compacted zone has an R_C = 61%. The embankment zone has a total width of 72 m, a length of 18 m, and a height of 5 m, with each of the four zones being a square measuring 18 m by 18 m. Field test includes embedded soil stiffness measurements, dynamic cone penetration tests, and field density tests. Laboratory tests include the Proctor tests and modified oedometer tests to facilitate comparisons with comprehensive tests. The field compaction criteria determine based on the Proctor test results, and field density tests assess the compliance with the criteria for each layer. The evaluation of density under field conditions is presented using comprehensive test methods, including DCPI and shear wave velocity, and compared with a physical-inspired model derived from a modified oedometer test. Results show an increase in measurements corresponding to strength changes at different compaction efforts and an increase with depth due to higher stress distribution. Finally, the depth-dependent shear wave velocity profile reveals trends consistent with the exponential compaction model predictions and target relative densities. These findings suggest that shear wave velocity is a suitable method for evaluating embankment layers when compared with comprehensive test data and highlight the potential of this approach for long-term monitoring applications.

KEYWORDS: Shear wave velocity, Relative density, Relative compaction, Exponential compaction model.

1 INTRODUCTION

Field compaction is a primary consideration for ensuring the long-term stability of civil structures subject to monitoring. Early studies have prompted the development of geological and geotechnical investigation techniques to quantitatively assess the degree of compaction and facilitate its management (Kim et al. 2014; Lee et al. 2021; Duddu and Chennarapu 2022; Kim et al. 2023; Kim et al. 2024a; Kim et al. 2024b; Park et al. 2024). However, the suggested method was limited in its applicability to long-term monitoring of embankment layers. Furthermore, the importance of the seismic design highlights the need to incorporate small-strain stiffness parameters. In this context, shear wave monitoring is essential for evaluating the small-strain stiffness and providing design parameters for civil structures (Kim et al. 2024c).

In this study, the embankment layers were compacted layer by layer and evaluated using shear wave velocity monitoring, dynamic cone penetration DCP tests, and field density measurements. The embankment layers were compacted at four different relative compaction values R_C: non-compacted, 80 %, 90 %, and 95 %. The field density test results were compared with the target density values, which were defined based on the concepts of relative compaction and relative density. The DCP and shear wave velocity were compared with the relative densities derived from an exponential compaction model using a modified oedometer system. This study used field measurements combined with laboratory experiments and depth models, providing a simple but robust method for examining the evolution of density in embankment layers.

2 TEST MOTHOD

2.1 *Site description*

Figure 1 shows a test bed divided into four zones with target relative compactions: R_C = non-compacted, 80%, 90%, and 95%. The test bed had dimensions of 18 m × 18 m square to ensure a uniform stress distribution. Then, a single-drum roller with a 2.3 m steel drum and a dynamic load of 107.02 kN at 30 Hz was used to compact the 30 cm-thick embankment layers. Bender elements were installed at -0.3 m to monitor shear wave velocity during compaction.
The number of roller passes applied to each embankment zone was determined based on the modified Proctor test conducted in the laboratory. The detailed criteria are discussed in Section 2.3.

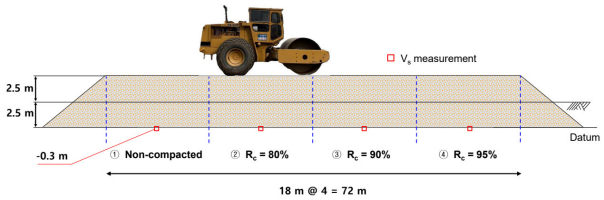

Figure 1. Illustration of test bed. The total height H = 5 m, and the total length L = 72 m.

2.2 *Test material*

Figure 2 shows the grain size distribution curve of the soil used in the embankment. The particle size characteristics included D_{10} = 0.07 mm, D_{30} = 0.29 mm, and D_{60} = 1.07 mm so that the coefficient of uniformity was C_u = 15.28, and the coefficient of curvature was C_c = 3.87. The specific gravity of the specimen is G_s = 2.70 (ASTM-D854, 2023). Based on the Unified Soil Classification System (USCS), the soil was classified as a poorly graded sand SP (USCS, ASTM D421 2021). The maximum dry unit weight was $\gamma_{d,max}$ = 19.48 kN/m³, with a minimum void ratio of e_{min} = 0.36 from the modified Proctor test (ASTM D1557 2021), and e_{min} = 0.51 from the maximum index density test (ASTM D4253 2019). The minimum dry unit weight was $\gamma_{d,min}$ = 12.80 kN/m³, with a maximum void ratio of e_{max} = 1.07 (ASTM D4254 2016).

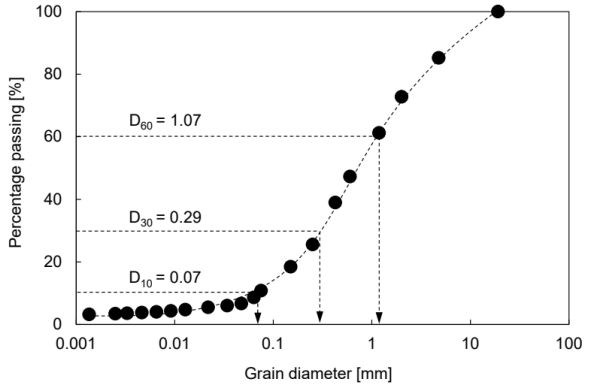

Figure 2. Grain size distribution curve of embankment material.

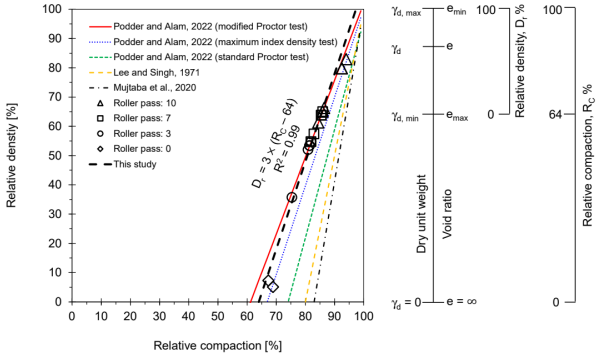

Figure 4. Relationship between relative density and relative compaction.

2.3 *Compaction criteria*

The compaction criteria were established based on the results of the modified Proctor test, which was performed to determine the maximum dry density $\gamma_{d,max}$. Figure 3a shows the results of the modified Proctor test with $\gamma_{d,max}$ = 19.5 kN/m^3 and an optimum moisture content OMC = 8.23%.

Then, we constructed another set of embankment layers to determine the actual number of roller passes required. Figure 3b shows the field dry density $\gamma_{d,field}$ changes with the number of roller passes. Following this criterion, we selected the number of roller passes for the four embankment zones (R_C = 61%: non-compacted, R_C = 80%: roller passes = 3, R_C = 90%: roller passes = 7, R_C = 95%: roller passes = 10).

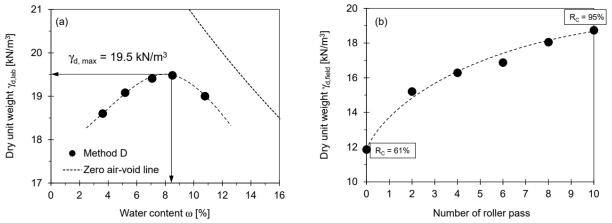

Figure 3. Compaction criteria based on pilot test bed dimensions: 3 m × 20 m × 0.9 m (width × length × height). (a) Modified Proctor curve using compaction method, and (b) dry unit weight according to roller passes.

2.4 *D_r and R_c concepts*

A construction sites in the field, relative compaction is widely used for compaction management, whereas at the laboratory scale, tests are familiar with relative density. In this context, we compare both concepts of the relative compaction and relative density. A strong relationship between D_r and R_C was observed based on the test results. Figure 4 illustrates the concepts of D_r and R_C, and Equation (1) presents the representative correlation line proposed in this study. Hence, we reasonably estimate the relative density from relative compaction.

$$D_r = 3 \times (R_C - 64)\ [\%] \quad (1)$$

where, D_r is the relative density, and R_c is the relative compaction.

2.5 *Modified oedometer system*

Figure 5 shows the modified oedometer system with inner diameter of D = 150 mm and a height of H = 76 mm. The thick-walled cylinder theory confirms that the cell thickness machined at t = 25 mm maintains the zero-lateral strain conditions at maximum vertical effective stress σ'_v = 500 kPa. Remolded relative densities D_r = 45%, 90%, and 85% with average water content ω = 11.16% (from the field density test) were chosen to evaluate the compaction characteristics of the embankment layers. This study monitors the load–deformation response at each static loading step using digital gauges (C112XB, Mitutoyo Corporation; resolution = 0.001 mm), and measures the shear wave velocity using a bender element.

The source bender element receives a square wave signal of 20 Hz frequency and 10 V_{pp} from a signal generator (Agilent 33220A) and the wave travels through the porous media to reach the receiving bender element. Received signals from the bender element pass through a filter-amplifier (Krohn-Hite 3944), which removes low-frequency noise below 500 Hz and amplifies the signal (gain = 20 dB), before being visualized and stored using an oscilloscope (Keysight DSO-X 3014A).

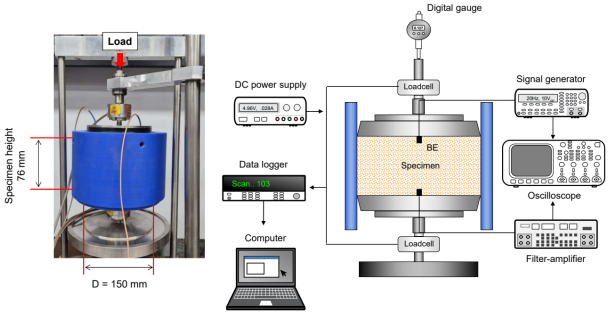

Figure 5. Schematic of modified floating-ring oedometer system. The D: H = 2:1 minimize soil-wall friction. Bender elements BE and load cells mounted in the top and bottom caps measure shear wave velocity and axial load.

2.6 *Field-scale measurements*

The field-scale measurements include the Dynamic Cone Penetration DCP test and the embedded soil stiffness measurement system. The DCP test follows the ASTM D6951-03 procedure and application dimensions. An embedded soil stiffness system equipped with bender elements measures the shear wave velocity at each embankment height. The measurement procedure follows the same method described in Section 2.5.

3 TEST RESULTS

3.1 *Modified oedometer system response*

3.1.1 *Evaluation D_r using shear wave velocity*

Figure 6a shows the modified oedometer test results (dashed lines from the laboratory data) along with the field measurements represented by symbols. The estimation line for relative density D_r = 15% was calculated based on other relative density data using the β-exponent and α-factor in the parameter space. Overall, the shear wave velocity increases as the number of roller passes increases.

Figure 6b presents the α-factor and β-exponent from the modified oedometer test. The results were within the typical range for sand. The inset trendline was suggested by Ramirez et al. (2023). Table 1 summarizes the parameters of the modified oedometer system.

Table 1. This is a table caption.

Relative density D_r [%]	Shear wave factors	
	α	β
15 (Estimate)	89.0	0.206
45	107.5	0.191
60	115.2	0.188
85	130.3	0.175

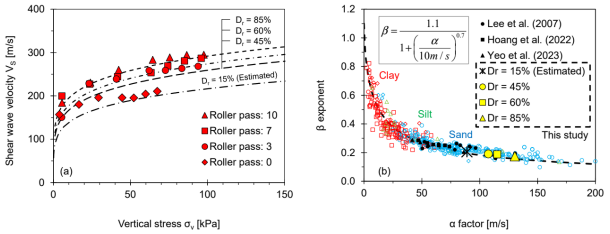

Figure 6. Shear wave velocity analyses: (a) comparison of shear wave velocities obtained from laboratory (dashed line) and field (symbol) measurements, and (b) α and β parameter space obtained through modified oedometer test

3.1.2 *Exponential compaction model*

Based on the oedometer response results, the effective stress with depth can be estimated by considering the relative density (See more details in Park and Santamarina 2020; Lyu et al. 2021):

$$\frac{d\sigma_z'}{dz} = G_s\gamma_w\left[\frac{1+\omega}{1+e_z}\right] \quad (2)$$

where z is the depth, G_s is the specific gravity of the soil particles, e_z is the void ratio by the depth, ω is the water content, and γ_w is the unit weight of water (γ_w = 9.81 kN/m^3).

3.2 *Field density test and DCP*

Figure 7a shows the field density test results with varying numbers of roller passes. The cases with 3 and 10 passes meet the target relative density D_r, indicated by dashed lines, while 7 passes fail to meet the target D_r. Additionally, the case with 0 passes results in a relative density of nearly 0%, which is considered physically meaningless.

Figure 7b shows the dynamic cone penetration DCP test results with varying numbers of roller passes. The DCP test is a sensitive indicator of the target ground and provides a complementary method for evaluating embankment layers.

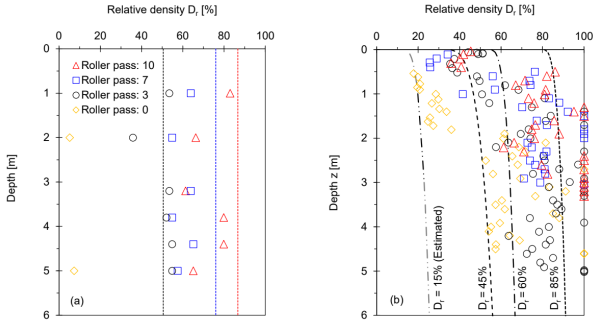

Figure 7. Field test results with varying number of roller passes (a) Field density test, and (b) DCP test.

3.3 *Shear wave velocity profiles*

The shear wave velocity profiles can be established by linking the oedometer test results with the depth-dependent model from Equation (2). Figure 8 shows the shear wave velocity profiles with varying numbers of roller passes. The shear wave measurements, denoted by symbols, follow each estimation line. Hence, we find that the relative density of the embankment layers in the compacted zones (roller passes: 3, 7, and 10) exceeds D_r = 60%, while the non-compacted zone is close to D_r = 15%. This study links field-measured shear wave velocity with constitutive parameters obtained from laboratory testing and an exponential compaction model to estimate the evolution of relative density with depth. The proposed method demonstrates good agreement with the observed trends in the relative density within the embankment layers.

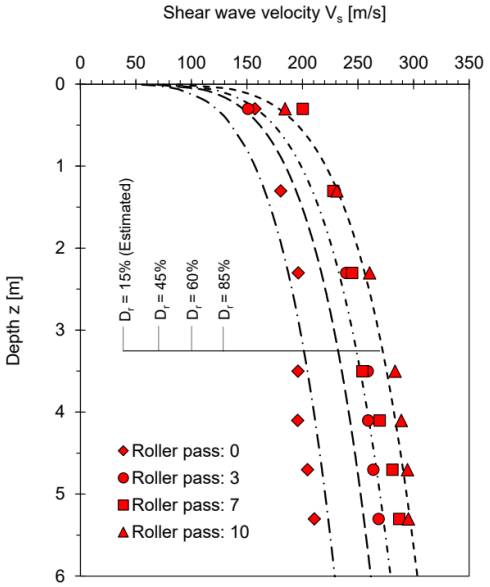

Figure 8. Shear wave velocity V_s profiles from embankment layers.

4 CONCLUSIONS

This study evaluated the relative density of the embankment layers using three distinct methods: field density test, dynamic cone penetration DCP test, and shear wave velocity V_s. The results followed the target relative density, and it was possible to track their changes. The main conclusions are as follows:

- The strong linear correlation between relative density D_r and relative compaction R_C facilitates interconversion, bridging field observations with laboratory interpretations.
- The shear wave velocity profiles play a complementary role to the DCP test, providing corroborative information for evaluating the target embankment layers.

Shear wave velocity as a function of depth offers a robust indicator for tracking changes in relative density, plays a critical role in long-term monitoring, and provides in-situ stiffness evaluation for seismic design.

5 ACKNOWLEDGEMENTS

This work was supported by the National Research Foundation of Korea (NRF) grant funded by the Korea government (MSIT) (No. NRF-2021R1A5A1032433).

6 REFERENCES

ASTM, 2003. Standard test methods for use of the dynamic cone penetrometer in shallow pavement applications, ASTM International Standards, D6951-03.

ASTM 2016. Standard test methods for minimum index density and unit weight soils and calculation of relative density, ASTM International Standards, D4254-16.

ASTM 2019. Standard test methods for maximum index density and unit weight of soils using a vibratory table, ASTM International Standards, D4253-00.

ASTM, 2021. Standard test methods for laboratory compaction characteristics of soil using modified effort, ASTM International Standards, D1557-12.

ASTM 2021. Standard practice for dry preparation of soil samples for particle-size analysis and determination of soil constants, ASTM International Standards, D421-85.

ASTM 2023. Standard test methods for specific gravity of soil solids by water pycnometer, ASTM International Standards, D854-02.

Duddu, S. R., & Chennarapu, H. 2022. Quality control of compaction with lightweight deflectometer (LWD) device: a state-of-art. International Journal of Geo-Engineering 13, 6.

Kim, K. -S., Fratta, D., and Wen, H. 2014. Field measurements for the effectiveness of compaction of coarse-grained soils. KSCE Journal of Civil Engineering 18, 497–504.

Kim, M., Lee, C., Kim, J. -U., and Choo, H. 2023. Use of shear wave velocity for assessing engineering properties of compacted bentonite after swelling. Sci Rep 13, 15705.

Kim, N., Park, G., Kim, S. Y., Lee, J. -S., and Park, J. 2024a. Physics-inspired geophysical assessment of liquefaction potential in Pohang, South Korea. Acta Geotech. 19, 1799–1813.

Kim, N., Lee, J. -S., Park, G., Yoo, Y., and Park, J. 2024b. Evolution of relative density and shear wave velocity in non-compacted embankment layers: Geological long-term monitoring. Engineering Geology 340, 107674.

Kim, N., Lee, J. -S., Yoo, Y., Kim, J., and Park, J. 2024c. Embedded type new in-situ soil stiffness assessment and monitoring technique. Smart Structures and Systems 34, 33–40.

Lee, J. -S., Tutumluer, E., and Hong, W. -T., 2021. Stiffness evaluation of compacted geo-materials using crosshole-type dynamic cone penetrometer (CDP), rPLT, and LFWD. Construction and Building Materials 303, 124015.

Lyu, C., Park, J., and Santamarina, J. C. 2021. Depth-Dependent Seabed Properties: Geoacoustic Assessment. J. Geotech. Geoenviron. Eng. 147, 04020151.

Park, J., and Santamarina, J. C. 2020. The critical role of pore size on depth-dependent microbial cell counts in sediments. Sci Rep 10, 21692.

Park, K., Kim, Y. J., Chen, J., and Nam, B. H. 2024. InSAR-based investigation of ground subsidence due to excavation: a case study of Incheon City, South Korea. International Journal of Geo-Engineering 15, 26.

Salva Ramirez, M., Park, J., Terzariol, M., Jiang, J., and Santamarina, J.C. 2023. Shallow Seafloor Sediments: Density and Shear Wave Velocity. J. Geotech. Geoenviron. Eng. 149, 04023022.